Visibility estimation in point clouds with variable density

Pierre Biasutti, Aurélie Bugeau, Jean-François Aujol, Mathieu Brédif

Visibility estimation in point clouds with variable density

P. Biasutti[1,2,3], A. Bugeau[1], J-F. Aujol[2], M. Brédif[3]
[1]*Univ. Bordeaux, LaBRI, INP, CNRS, UMR 5800, F-33400 Talence, France*
[2]*Univ. Bordeaux, IMB, INP, CNRS, UMR 5251, F-33400 Talence, France*
[3]*Univ. Paris-Est, LASTIG GEOVIS, IGN, ENSG, F-94160 Saint-Mandé, France*
{*pierre.biasutti, aurelie.bugeau*}*@labri.fr, jean-francois.aujol@math.u-bordeaux.fr, mathieu.bredif@ign.fr*

Keywords: 3D point cloud, visibility, visualization, LiDAR, dataset, benchmark

Abstract: Estimating visibility in point clouds has many applications such as visualization, surface reconstruction and scene analysis through fusion of LiDAR point clouds and images. However, most current works rely on methods that require strong assumptions on the point cloud density, which are not valid for LiDAR point clouds acquired from mobile mapping systems, leading to low quality of point visibility estimations. This work presents a novel approach for the estimation of the visibility of a point cloud from a viewpoint. The method is designed to be fully automatic and it makes no assumption on the point cloud density. The visibility of each point is estimated by considering its screen-space neighborhood from the given viewpoint. Our results show that our approach succeeds better in estimating the visibility on real-world data acquired using LiDAR scanners. We evaluate our approach by comparing its results to a new manually annotated dataset, which we make available online.

1 Introduction

Over the past decade, the use of 3D point clouds as an alternative to meshes has been constantly growing. A 3D point cloud simply consists in 3D positions, sometimes associated with supplementary information such as its color, reflectance or normal. It can be considered as a sampling of continuous surface, providing a simpler representation than the full topology.

The estimation of the visibility of a point cloud consists in assigning a label to each point of the scene: visible if the point lies on an object that is directly visible from a given viewpoint, non-visible otherwise (Fig. 1). This task is a typical step for various applications in computer graphics such as in surface reconstruction (Zach et al., 2007; Shalom et al., 2010; Berger et al., 2017) in which estimating and removing points that are not visible from a given point of view improves the interpolation and the approximation of the surface to recover. In point cloud rendering and visualization (Pintus et al., 2011; Bouchiba et al., 2017), the estimation of the visibility enables better rendering performances as well as an improvement of the scene understanding. For both application scenarios, the existing methods (Zach et al., 2007; Shalom et al., 2010; Berger et al., 2017; Pintus et al., 2011; Bouchiba et al., 2017) strongly rely on strict sampling assumptions (Berger et al., 2017) (*e.g.* on point clouds with constant density in terms of number of points per cubic meters).

a. b. c. d.

Figure 1: Illustration of the visibility problem. (a) an optical image corresponding to a view point, (b) the 3 main structures of the scene, (c) the projection of the acquired point cloud seen from the same view point with same colors as in (b), (d) the visibility errors brought by the projection (red points should not be visible).

Recently, the development of acquisition systems designed for acquiring urban scenes has been increasing. In particular, Mobile Mapping Systems (MMS) equipped with LiDAR (Light Detection And Ranging) (Paparoditis et al., 2012; Geiger et al., 2013; Maddern et al., 2017) have been widely used to survey cities, road, highways, etc. Those campaigns have resulted in the production of large, unorganized point clouds that provide precise 3D representations of the

urban environment. Due to the acquisition method, these point clouds present high variation in their sampling and density. Most modern MMS also embed additional materials, mostly optical images, which provide complementary information on the scene. The multimodal aspect of these datasets may be leveraged to improve detection, classification and prediction techniques in urban environments (Benenson et al., 2014; Eigen et al., 2014). Therefore, the fusion and the registration of LiDAR and optical data became critical as the use of multi-modal data definitely increases performances of classification/prediction algorithms. Most of the recent related works strongly rely on good visibility estimates (Mastin et al., 2009; Guislain et al., 2017).

The majority of actual LiDAR/optical registration techniques that use visibility rely on estimation techniques that were built for point clouds with strict sampling assumptions that are not met by the LiDAR data on which they operate. On the other hand, point cloud rendering and surface reconstruction methods presented above are not designed to perform on point clouds with variable density. However, the quality of the visibility estimation is a crucial preprocessing step for multi-modal fusion applications as it drastically lowers the ambiguities from one modality to another. This work aims at studying a new method for estimating the visibility in point clouds without constant density acquired via MMS to improve the data fusion.

The paper contribution is threefold: first, we propose a novel approach for the visibility estimation in a point cloud that is robust to high density variations. This method is designed to be fully automatic and to perform well on any types of 3D point clouds. The second contribution of this article is a new visibility dataset of over 1 million annotated points for testing the performances of visibility estimation methods. This dataset, as well as the code for our method, are made publicly available online. The third contribution of this dataset is a full numerical and visual comparison between our method and other state-of-the-art methods.

The paper is organized as follows: first, a brief overview of the related work is presented. Then, the methodology of the method is explained. Finally, evaluation and results are shown and a conclusion is drawn.

2 Related works

There has been many contributions to the state-of-the-art techniques for the estimation of the visibility of a point cloud given a certain viewpoint. In this section, we briefly overview the methods that are most relevant to our work.

Surface reconstruction based One intuitive way to compute the visibility of a point cloud is to reconstruct the surface. Indeed, the projection of the surface as a depth map may be used to estimate which points are not visible. Some methods do not require prior knowledge of the visibility and can therefore be used for visibility estimation. *Surface smoothness* approaches (Lipman et al., 2007; Xiong et al., 2014) approximate the surface by locally defining operators that weigh surrounding points in order to estimate the local surface. This constrains the reconstructed surface to fit the point cloud as close as possible while ensuring a certain level of smoothness and preserving sharp features. To deal with large amounts of missing data, *Volume smoothness* techniques (Tagliasacchi et al., 2011; Huang et al., 2013) exploit the prior of smooth variation of the volume of the reconstructed surface. Unfortunately, these methods are based on strong prior of uniform sampling of the point cloud, which is not suitable for MMS LiDAR point clouds. *Primitive based* methods (Schnabel et al., 2009; Lafarge and Alliez, 2013) aim at fitting geometric shapes (*i.e.* planes, spheres, cylinders, boxes, etc.) in order to reconstruct the scene. However, the complex shapes that can be met in real world scene often jeopardize the results of such methods. Finally, *Global regularity* approaches (Li et al., 2011a; Li et al., 2011b; Monszpart et al., 2015) take advantage of the repeatability of certain parts of the scene. These methods have shown great strength for the reconstruction of individual regular shapes such as facades or roads but underperform on realistic complete scenes. Although each technique provides satisfying results on specific scenarios, surface reconstruction is a difficult problem, which often requires additional information, such as normals, sufficiently dense input and uniform sampling.

Convex hull based Some methods estimate the visibility based on the local geometry of the 3D point cloud. Based on the raw point cloud (*i.e.* only 3D positions), (Katz et al., 2007) proposes an approach for estimating which part of the point cloud is not self-occluded given a certain viewpoint. This method admits to perform better on closed shapes. A spherical inversion is performed on the point cloud. The convex hull of the inverted point cloud augmented by the viewpoint position is computed. Then, points that are lying on the convex hull are considered visible, and the rest of the point cloud as non-visible. The acceptance of concave features is tuned by the

sphere radius, which is a global parameter so that this method strongly relies on a uniform sampling of the point cloud. Later, this method was improved to handle small changes in the sampling corresponding to noisy acquisitions (Mehra et al., 2010), but still relies on constant density in the point cloud. Moreover, the computational cost of the convex hull (Barber et al., 1996) can rapidly increase depending on the wanted concavity. Finally, (Katz et al., 2007; Mehra et al., 2010) are both designed to perform on point clouds that represent closed shapes, acquired from all directions, which is not realistic in urban scenarios where MMS are not able to scan all surfaces.

Likelihood based Different methods aim at estimating the likelihood of a point to be visible given a point of view, by considering its neighborhood. The most common methods rely on the estimation of visibility cones in screen-space (Shalom et al., 2010), and more recently (Pintus et al., 2011). For each point, a visibility cone is estimated, where the apex of the cone is the given viewpoint. The aspect of the cone is directly related to the visibility. Thus, a point that belongs to a wide cone is more likely to be visible than a point that belongs to a narrow cone. However, the threshold on how open a cone should be in order to consider the point visible strongly depends on the point cloud, and can be hard to set.

In this paper, we propose an automatic screen-space method for estimating the visibility of points in a point cloud given a viewpoint. This method makes no assumptions on the sampling or the density of the point cloud and can therefore performed on any point cloud.

3 Visibility estimation method

The first contribution of this paper is a method for estimating visibility in a 3D point cloud that is robust to high sampling variations.

As illustrated in Fig. 2, points from two objects located at different distances from the given viewpoint overlap in the image plane once projected. In this context, a point is visible only if it lies on the closest object and occluded otherwise. From this observation, we propose an algorithm that considers the neighborhood of a point in screen-space in order to estimate whether this point lies on the closest object or not. The algorithm consists in 4-steps detailed hereafter.

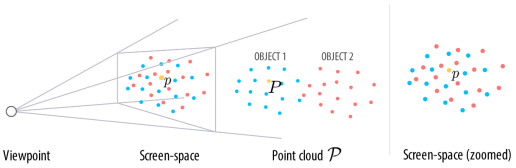

Figure 2: Illustration of notations in 3D and in the screen-space. Blue points corresponds to the points lying on the closest object while red points lies on the farthest object. Although the blue points and red points are well separated in 3D, they overlap in screen-space.

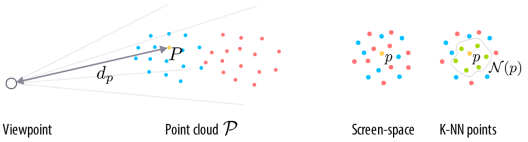

(a) (b)

Figure 3: Illustration of the depth and of the closest points. (a) d_p corresponds to the depth between P and the center of the viewpoint, (b) shows an example of the N closest points in screen-space ($N = 6$).

Projection to screen-space Let $\mathcal{P}$ be a 3D point cloud, and Φ a viewpoint such that any 3D point $P = \begin{bmatrix} x \\ y \\ z \end{bmatrix} \in \mathcal{P}$ can be projected as a point $p = \begin{bmatrix} x \\ y \end{bmatrix} \in \mathcal{P}_\Phi$ in the image plane of the viewpoint Φ. The relation between P and p is illustrated on Fig. 2. We also define d_p as the depth of the point p. It corresponds to the 3D Euclidean distance between P and the center of the viewpoint as illustrated Fig. 2(a).

Neighbors computation We define $\mathcal{N}(p)$ as the set of the N nearest neighbor points of p in the image plane as explained in Fig. 3(b) The $\mathcal{N}(p)$ set can be computed using any K-NN alogrithm with a Euclidean distance. The use of the K-NN algorithm defined in (Friedman et al., 1977) ensures logarithmic computation time while being parallelizable.

Visibility estimation For each point, we want to determine if it lies on the object in its neighborhood that is the closest to the viewpoint. If so, we can consider it as visible. To that end, we compare its position to the closest and the farthest point of its neighborhood. We define the visibility of each point as follows:

$$\alpha_p = e^{-\frac{\left(d_p - d_p^{min}\right)^2}{\left(d_p^{max} - d_p^{min}\right)^2}} \quad (1)$$

where

$$d_p^{min} = \min_{q \in \mathcal{N}(p)} d_q, d_p^{max} = \max_{q \in \mathcal{N}(p)} d_q$$

The visibility estimation of each point $p \in \mathcal{P}_\Phi$ is now given by $\alpha_p \in [0,1]$, where $\alpha_p = 0$ means that p is occluded and $\alpha_p = 1$ means that p is surely visible.

Binarization The visibility of a point cloud being a binary notion, we propose the following binarization of α_p:

$$\hat{\alpha}_p = \begin{cases} 1 & \text{if } \alpha_p \geq \bar{\alpha} \\ 0 & \text{otherwise.} \end{cases} \quad (2)$$

with $\bar{\alpha} = \frac{1}{Card(\mathcal{P}_\phi)} \sum_{p \in \mathcal{P}_\phi} \alpha_p$ the mean of the estimated visibilities. Note that various $\bar{\alpha}$ values have been tested such as $\bar{\alpha} = 0.5$ or the median value of the estimated visibilities as discussed Section 5. However, in our experiments on LiDAR data, the mean value remains the best threshold. When point clouds have constant densities, $\bar{\alpha} = 0.99$ appears to be more adequate.

4 Visibility estimation dataset for LiDAR point clouds

The evaluation of visibility estimation techniques has mostly been done either by visual analysis or by comparison to degradated synthetic models. In (Shalom et al., 2010; Katz et al., 2007), visual results are displayed to show the qualitative performances of each algorithm. In (Mehra et al., 2010), small degradations on synthetic model are applied in order to build groundtruths. Although these methods of evaluation provide convincing results, they do not provide complete and objective quantitative measures on real data. Real data, such as LiDAR, differ from synthetic data in two aspects. The first difference is that the point cloud density is highly variable on real data depending on the distance to the sensor, while constant on synthetic data. The second one is that real urban data only acquire partial representations of each object of the scene as the sensor does not see objects from every possible viewpoints. On the other hand, the synthetic data presented in the related works (Shalom et al., 2010; Katz et al., 2007; Mehra et al., 2010) are always complete 3D objects, which can be seen from any viewpoint. To our knowledge, we give here the first annoted dataset on real urban LiDAR data, which makes the second contribution of this paper.

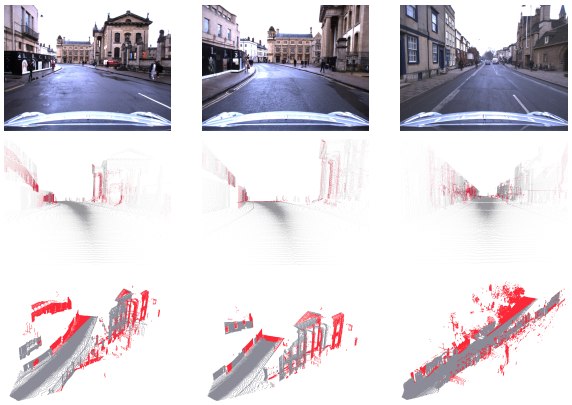

Figure 4: Overview of the proposed dataset. First row: optical image corresponding to each viewpoint. Second row: point cloud once projected in the image domain, where red pixels correspond to occluded points. Third row: 3D visualization of each point cloud, with the same color code than in the second row.

4.1 Overview of the dataset

We propose a manually annotated dataset containing over a 1 million points with the label 1 or 0 depending on if the points are visible or not. This dataset has been obtained by manually labeling 3 point clouds acquired by the RobotCar system (Maddern et al., 2017) at different locations, in urban environment. Two of these point clouds are acquired several meters from one another in order to test the stability of visibility estimation methods. The third point cloud corresponds to another location and covers a much wider area which enables testing the limit of methods in case of large distances ($>$ 100m).

Annotations were done manually by comparing the projections of the point clouds to the optical images acquired at the same viewpoints. Fig. 4 presents an overview of the produced dataset. The first row illustrates each scene as acquired from the optical sensor at each viewpoint. The second row shows the projections of each point cloud in the image domain (with the calibration matrices provided by the Robotcar dataset (Maddern et al., 2017)), where occluded points are highlighted in red. Finally, the third row shows a 3D visualization of each point cloud, with same color code than above. It illustrates the amount of points to be processed as well as the size of the scenes. The statistics of the dataset are summed up in Table 1. The dataset proposes different levels of visible / occluded points, as well as different size of the scene.

This dataset is publicly available online[1]. The

[1] *http://www.labri.fr/perso/pbiasutt/Visibility/*

Table 1: Content of the visiblity estimation dataset

	Points	Visibility	Farthest point	Size
Scene #1	337384	55.5%	75.8m	20.6Mb
Scene #2	247682	57.0%	54.3m	15.1Mb
Scene #3	463531	65.9%	179.2m	28.3Mb
Total	1048597	59.46%	-	64Mb

archive contains 3 text files in the *.xyz* format that correspond to each point cloud. In each file, a line corresponds to $[x, y, z, u, v, label]$ where x, y, z are the 3D coordinates of the point, u, v are the 2D coordinates of the point when projected into ϕ and *label* is the visibility label (0 for occluded points, 1 for visible points). To ensure good understanding of each of the 3 scenes, we also provide the optical RGB image of size 1280×960px associated to each viewpoint.

5 Experiments & Results

In order to evaluate the performances of our visibility estimation method, we first perform a full numerical and visual comparison between our method and other state-of-the-art methods on (1) the proposed visibility dataset, (2) a point cloud with constant density. Next, we show application of our method to data fusion by performing point cloud colorization from RGB images. All the algorithms are run on Matlab 2018a with a 3.5Ghz CPU.

5.1 Evaluation on the Visibility Estimation Dataset

Using our new annotated dataset, we propose an evaluation with two state-of-the art methods, and with our proposed model, against a groundtruth. For each method, we set all the parameters to its optimal value (*e.g.* the parameters that gives best results against the groundtruth). In our case, we set $N = 75$ and we detail results for different $\bar{\alpha}$ values. We measure the efficiency of each method by computing the following metric:

$$S(\mathcal{P}) = \frac{1}{\text{Card}(\mathcal{P})} \sum_{P \in \mathcal{P}} \alpha_p \times \text{GT}_p \qquad (3)$$

where GT_p corresponds to the annotation of the point P (0 or 1, occluded or visible respectively). This metric aims at capturing the percentage of correctly labeled points provided by each method. The results of this evaluation are displayed in Table 2.

Table 2 demonstrates that our algorithm outperforms each compared methods for the 3 scenes. The best scores are obtained by setting the threshold $\bar{\alpha}$ equal to the mean of visibility estimations for our method. This observation is explanable. Indeed, as mentionned above, LiDAR aquisitions only capture pieces of the scene. Thus, objects are represented by one of their face only which makes them well separated from one another. In this sense, when an object overlaps an other in screen-space, the mean of the visibility estimations usually represents the visibility of a point that would be in between those two objects. If a point has a visibility estimation above this threshold, it is likely to fall on the closest object, otherwise, it is occluded. Therefore, the mean value can be used when working on LiDAR point clouds because of the way objects are separated from one another, making the method fully automatic in this context.

We also demonstrate that our method operates faster than any other tested method with the ability of treating the whole dataset in less than a second. Moreover, the code is run on a single CPU. Among the 4 steps of the algorithm, the computation of the K-NN is the most time consuming (about 86% of the total running time). Therefore, one can expect much faster running times by operating on GPU with parallel implementation of the K-NN algorithm.

The problem of visibility estimation is a classification problem with two classes: visible and occluded points. Therefore, we enrich our evaluation by com-

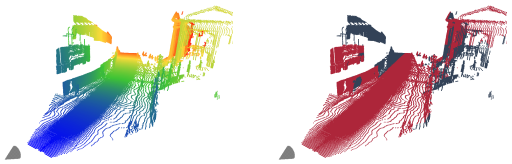

(a) Point cloud (b) Ground truth

(c) HPR d. Proposed model

Figure 5: Results of visibility estimation on the first scene of our visibility estimation dataset.. (a) the point cloud where the heat of the color is proportional to the depth, (b) is the annotated point cloud (red: visible, grey: non-visible), (c) HPR result and (d) our result. The result brought by HPR estimates too many visible points, whereas our method provides a result that is very close to the groundtruth.

Table 2: Comparison of the scores of two state-of-the art and our visibility estimation methods on our visibility estimation dataset

Threshold	**HPR** (Katz et al., 2007) optimal	**Cone** (Pintus et al., 2011) optimal	**Ours** $\bar{\alpha} = 0.5$	**Ours** α_p median	**Ours** α_p mean
POV #1	74.09%	68.76%	90.15%	86.35%	**90.96%**
POV #2	69.09%	61.68%	86.95%	86.78%	**88.39%**
POV #3	81.55%	75.58%	82.21%	76.35%	**83.75%**
Average	74.91%	68.67%	86.43%	83.16%	**87.70%**
Total time	7.82s	1.53s	**0.91s**	1.03s	**0.91s**

Table 3: Comparison of the different methods for point cloud visibility classification

Threshold	**HPR** (Katz et al., 2007) optimal	**Cone** (Pintus et al., 2011) optimal	**Ours** $\bar{\alpha} = 0.5$	**Ours** α_p median	**Ours** α_p mean
True-positive	89.54%	85.16%	**95.45%**	78.31%	88.23%
False-positive	18.84%	17.78%	10.78%	**3.66%**	5.15%
False-negative	6.26%	8.61%	**2.79%**	13.18%	7.14%
True-negative	54.47%	56.24%	72.45%	**90.80%**	86.93%
Accuracy	85.16%	84.27%	92.52%	90.94%	**93.44%**
F1-score	87.71%	86.59%	93.37%	90.29%	**93.49%**

puting typical classification metrics for each method and display them in Table 3. For each metric, the best scores are obtained using our method. In particular, our method with $\bar{\alpha} = 0.5$ maximizes the true-positives and minimizes the false-negatives. On the opposite, our method with $\bar{\alpha}$ as the median of the estimations maximizes the false-positives and true-positives. Once again, using our method with $\bar{\alpha}$ as the mean of the estimations provides a good tradeoff between true-positives/true-negatives and false-positives/false-negatives. On the other hand, (Katz et al., 2007) and (Pintus et al., 2011) tend to over-estimate the visibility of each point, resulting in many occluded points being label as visible. This is expressed by the very high percentage of false-positive. We computed accuracy and the F1-score of each method against the ground truth. For both, our method with $\bar{\alpha}$ as the mean of the estimation achieves, once again, the best results.

For the task of data-fusion, it is often preferable to discard the maximum of occluded points (Bevilacqua et al., 2017). Therefore, the number of false-positives has to be kept as low as possible. In this sense, our method provides very satisfactory results, especially using the $\bar{\alpha}$ as the mean of estimations when working on LiDAR data.

We conclude this evaluation on LiDAR data by a visual analysis of the results of the different methods. Fig. 5 shows the results of the visibility estimations visualized in 3D. For each result, the dark cone in the bottom left corner represents the viewpoint. Fig. 5(a) shows the point cloud colorized with the depth toward the viewpoint (cold colors for close points, hot colors for far points). Fig. 5(b) shows the annotated groundtruth for this scene, where red points are points that are visible from the viewpoint and dark points are supposed to be occluded. Fig. 5(c) and 5(d) are the results of HPR (Katz et al., 2007) and our method (with $\bar{\alpha}$ set as the mean of estimations) respectively. We can see that HPR (Katz et al., 2007) estimates too many points as visible points, especially on the closest points. On the opposite, our method succeeds in discarding occluded points, and provides a result that is very close to the groundruth.

We also illustrate these results as seen from the associated viewpoint in Fig. 6. For better understanding purpose, Fig. 6(a) shows an image acquired from the same viewpoint. In Fig. 6(b), we only display visible points of the groundtruth. Fig. 6(c) and 6(d) shows the results of HPR (Katz et al., 2007) and our method respectively. We can see once again that HPR (Katz et al., 2007) labels too many occluded points as visible and fails to distinguish foreground from background objects. This is mostly due to the fact that this scene presents very high variations of density. In particular, the center of the road concentrates a very high density of points as the sensor is close from the road. Therefore, the convex-hull has to be relaxed enough to fit this region of the point cloud, which leads to visual abberations on regions with lower density. Our method succeeds better results this scene, which demonstrates its robustness against high density variations.

(a) Optical image

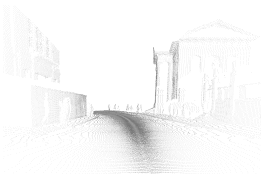

(b) Groundtruth

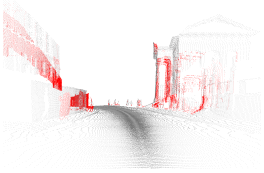

(c) HPR

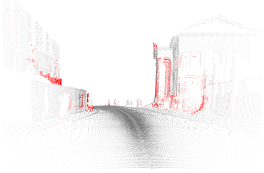

(d) Proposed model

Figure 6: Results of the visibility estimations on the first scene of the dataset in screen-space. (a) the optical image associated with the point of view, (b) visible points with respect to our annotation, (c) HPR result and (d) ours. Red points in (c) and (d) correspond to misestimated points.

Table 4: Comparison of the scores of the different methods on constant density point cloud

Threshold	**HPR** optimal	**Cone** optimal	**Ours** $\bar{\alpha} = 0.99$	**Ours** α_p mean
Score (Eq. (3))	**96.57%**	93.75%	95.23%	93.02%
True-positive	95.17%	88.63%	94.44%	**98.07%**
False-positive	1.15%	**0.88%**	2.14%	6.07%
False-negative	2.28%	5.37%	2.63%	**0.91%**
True-negative	97.82%	**98.33%**	95.95%	88.50%
Accuracy	**98.25%**	96.76%	97.56%	96.40%
F1-score	**98.23%**	96.59%	97.54%	96.57%

5.2 Evaluation on constant density point cloud

In previous section, we demonstrated that our method performs better than other methods for point clouds with high density variations. In this section, we aim at showing that our method remains competitive on constant density point clouds. The Stanford Bunny model is a point cloud (from the Stanford University CG Laboratory) that was created by merging 10 depth aquisitions of a real object and equalizing the density of the fused point cloud. The final point cloud is composed of 31655 points. As each depth acquisition only acquires points that are visible from a single viewpoint, we created a groundtruth by comparing the final point cloud to the points that were aquired at a certain viewpoint. Criterion (3) and classification metrics have been computed for our method and state-of-the-art methods. Results are displayed in Table 4.

Here, the point cloud is of constant density and represents a very smooth object as illustrated Fig. 7. This is a scenario that is perfectly adequate for the HPR algorithm, which shortly outperforms the two other methods. Our method underperforms only by about 1 percent but still remains very efficient on these types of data. Compared to the two other methods, our method fails on tangential points that are located at the boundaries of the projection of the object as it is presented on the last row of Fig. 7. This is mostly due to the fact that on tangential points, the neighborhood covers only a small area, thus the difference between foreground and background is hard to set. These artifacts are limited when using the mean of estimation as visibility threshold, but it increases false-positives. Table 4 also illustrates the classification metrics. We can see that all tested methods reach very good levels of accuracy and F1-score. Our method succeeds better when $\bar{\alpha} = 0.99$ than when using the mean value. Indeed, for complete object, there is no separation between foreground object and background object as was the case for LiDAR point clouds. Thus, only points with high likelihood should be kept to improve results, which justifies $\bar{\alpha} = 0.99$.

Finally, Table 4 assesses that all methods limit the appearance of false-positives while ensuring to gather as many visible points as possible. To that end, HPR and our method succeed the best true-positive/false-positive ratio, which is ideal for data-fusion purposes, as discussed in next section.

5.3 Example of application to data fusion

To conclude our experiments, we show the interest of our visibility estimation for the task of data fusion. Using the KITTI dataset (Geiger et al., 2013), we aim at colorizing a 3D LiDAR point cloud acquired in a street using only RGB images. Each point is projected in the image domain of the closest image (*e.g.* the image that was acquired at the closest position from the point). The point then takes the color of the pixel it projects into only if it is considered visible. Fig. 8 presents the result of the colorization on a point cloud composed of 3289533 points, and is colorized using 40 RGB images. Fig. 8(a) shows the colorization result where all points are considered visible. We can see that artifacts appear as the colors do not match the objects. This is particularly noticeable behind cars where the ground points take the color of the car. Fig. 8(b) displays the colorization result where the visibility is estimated using HPR (Katz et al., 2007). There, some artifacts appear behind cars as the convex-hull go through the glasses of the car. Moreover, this method discards many visible points on the ground and behind cars compared

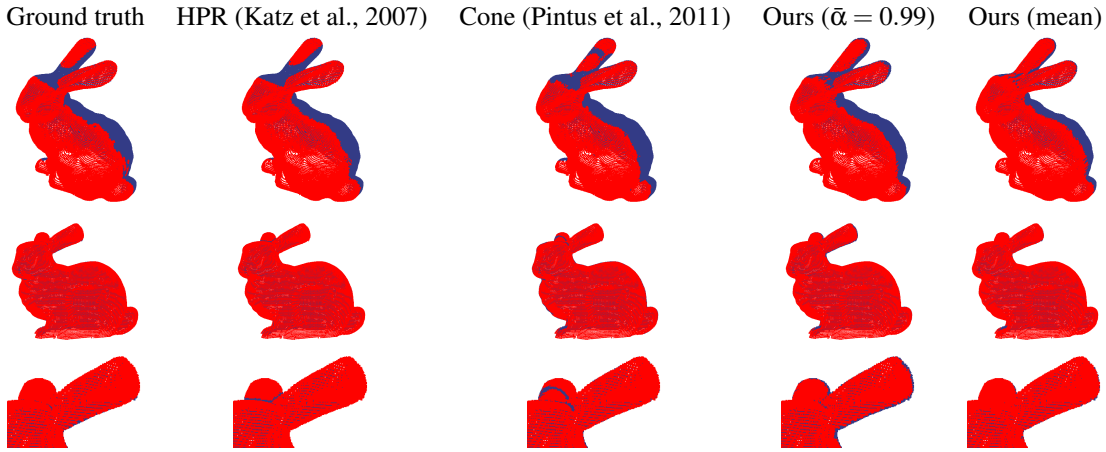

Figure 7: Visual comparison of the visibility estimation from different methods on a point cloud with constant and high density. Each column corresponds to one method. Rows are respectively: the results in 3D, the results in 2D (seen from the viewpoint), and a zoom of the 2D result focused on the ear region. The 3 methods succeed very well in estimating the visibility. Our methods lacks of precision for points that are tangent to the viewpoint as can be seen on the last row.

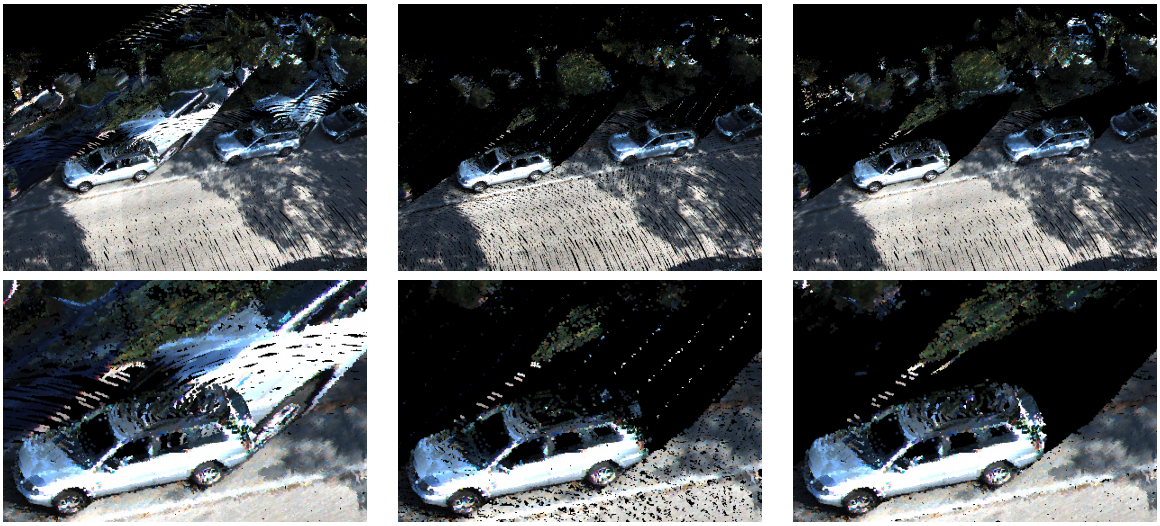

(a) (b) (c)

Figure 8: Comparison of the colorization of point clouds using RGB images. (a) colorization without any visibility information, (b) colorization with HPR (Katz et al., 2007) for the visibility estimation, (c) colorization with our visibility estimation method. The result provided by our method presents no artifacts on occluded areas, especially behind cars compared to the two other results.

to our method (about 17% less points are colorized). Fig. 8(c) presents the colorization result using our visibility estimation method. We can see that the artifacts behind cars have completely disappeared, while keeping most of the visible points. Finally, due to the number of points, the visibility estimation using HPR (Katz et al., 2007) for each viewpoint takes an average of 10.9 seconds whereas our method processes the point cloud at each viewpoint in about 1.2 seconds.

6 Conclusion & Perspectives

In this paper, we have proposed a novel method for the visibility estimation in a point cloud. Compared to other methods from literature, this method is very robust to high variations of density. By considering the closest neighbors of each point in screen-space, we defined a criterion in order to automatically determine the visibility of each point. We have also proposed a new annotated dataset for testing the efficiency of point cloud visibility algorithms on real LiDAR urban data. This dataset is composed of over

a million manually annotated points. Finally we have compared our method to state-of-the-art methods. We have validated that our method significantly outperforms existing methods on real urban data. Although our method was specifically designed for the estimation of visibility on point cloud with various density (such as LiDAR point clouds), we have also demonstrated that it still remains competitive on point clouds with constant density.

In the future, we would like to focus on the evaluation of our method against photogrammetric point clouds, for tasks such as view generation. We also would like to improve LiDAR / Optic fusion thanks to the visibility estimation.

7 Acknowledgement

This study has been carried out with financial support from the French State, managed by the French National Research Agency (ANR GOTMI) (ANR-16-CE33-0010-01). This project has also received funding from the European Union's Horizon 2020 research and innovation programme under the Marie Skłodowska-Curie grant agreement No 777826.

REFERENCES

Barber, C. B., Dobkin, D. P., and Huhdanpaa, H. (1996). The quickhull algorithm for convex hulls. *ACM Transactions on Mathematical Software*, 22(4):469–483.

Benenson, R., Omran, M., Hosang, J., and Schiele, B. (2014). Ten years of pedestrian detection, what have we learned? In *ECCV European Conference on Computer Vision*, pages 613–627.

Berger, M., Tagliasacchi, A., Seversky, L. M., Alliez, P., Guennebaud, G., Levine, J. A., Sharf, A., and Silva, C. T. (2017). A survey of surface reconstruction from point clouds. In *Computer Graphics Forum*, pages 301–329.

Bevilacqua, M., Aujol, J.-F., Biasutti, P., Brédif, M., and Bugeau, A. (2017). Joint inpainting of depth and reflectance with visibility estimation. *ISPRS Journal of the Photogrammetry, Remote Sensing and Spatial Information Sciences*, 125(1):16–32.

Bouchiba, H., Groscot, R., Deschaud, J.-E., and Goulette, F. (2017). High quality and efficient direct rendering of massive real-world point clouds. In *Eurographics Annual Conference of the European Association for Computer Graphics*, pages 1–6.

Eigen, D., Puhrsch, C., and Fergus, R. (2014). Depth map prediction from a single image using a multi-scale deep network. In *Advances in neural information processing systems*, pages 2366–2374.

Friedman, J. H., Bentley, J. L., and Finkel, R. A. (1977). An algorithm for finding best matches in logarithmic expected time. *ACM Transactions on Mathematical Software*, 3(3):209–226.

Geiger, A., Lenz, P., Stiller, C., and Urtasun, R. (2013). Vision meets robotics: The KITTI dataset. *IJRR International Journal of Robotics Research*, 32(11):1231–1237.

Guislain, M., Digne, J., Chaine, R., and Monnier, G. (2017). Fine scale image registration in large-scale urban LIDAR point sets. *CVIU Computer Vision and Image Understanding*, 157(12):90–102.

Huang, H., Wu, S., Cohen-Or, D., Gong, M., Zhang, H., Li, G., and Chen, B. (2013). L1-medial skeleton of point cloud. In *ACM Transactions on Graphics*, pages 65–72.

Katz, S., Tal, A., and Basri, R. (2007). Direct visibility of point sets. In *ACM Transactions on Graphics*, pages 24–36.

Lafarge, F. and Alliez, P. (2013). Surface reconstruction through point set structuring. In *Computer Graphics Forum*, pages 225–234.

Li, Y., Wu, X., Chrysathou, Y., Sharf, A., Cohen-Or, D., and Mitra, N. J. (2011a). Globfit: Consistently fitting primitives by discovering global relations. In *ACM Transactions on Graphics*, pages 52–64.

Li, Y., Zheng, Q., Sharf, A., Cohen-Or, D., Chen, B., and Mitra, N. J. (2011b). 2D-3D fusion for layer decomposition of urban facades. In *ICCV IEEE International Conference on Computer Vision*, pages 882–889.

Lipman, Y., Cohen-Or, D., Levin, D., and Tal-Ezer, H. (2007). Parameterization-free projection for geometry reconstruction.

Maddern, W., Pascoe, G., Linegar, C., and Newman, P. (2017). 1 year, 1000 km: The Oxford RobotCar dataset. *The International Journal of Robotics Research*, 36(1):3–15.

Mastin, A., Kepner, J., and Fisher, J. (2009). Automatic registration of LIDAR and optical images of urban scenes. In *CVPR IEEE Conference on Computer Vision and Pattern Recognition*, pages 2639–2646.

Mehra, R., Tripathi, P., Sheffer, A., and Mitra, N. J. (2010). Visibility of noisy point cloud data. *Computers and Graphics*, 34(3):219–230.

Monszpart, A., Mellado, N., Brostow, G. J., and Mitra, N. J. (2015). RAPter: rebuilding man-made scenes with regular arrangements of planes. In *ACM Transaction on Graphics*, pages 103:1–103:12.

Paparoditis, N., Papelard, J.-P., Cannelle, B., Devaux, A., Soheilian, B., David, N., and Houzay, E. (2012). Stereopolis II: A multi-purpose and multi-sensor 3D mobile mapping system for street visualisation and 3D metrology. *Revue française de photogrammétrie and de télédétection*, 200:69–79.

Pintus, R., Gobbetti, E., and Agus, M. (2011). Real-time rendering of massive unstructured raw point clouds using screen-space operators. In *Eurographics International Conference on Virtual Reality, Archaeology and Cultural Heritage*, pages 105–112.

Schnabel, R., Degener, P., and Klein, R. (2009). Completion and reconstruction with primitive shapes. In *Computer Graphics Forum*, pages 503–512.

Shalom, S., Shamir, A., Zhang, H., and Cohen-Or, D. (2010). Cone carving for surface reconstruction. In *ACM Transactions on Graphics*, pages 150–160.

Tagliasacchi, A., Olson, M., Zhang, H., Hamarneh, G., and Cohen-Or, D. (2011). VASE: Volume-Aware Surface Evolution for Surface Reconstruction from Incomplete Point Clouds. In *Computer Graphics Forum*, pages 1563–1571.

Xiong, S., Zhang, J., Zheng, J., Cai, J., and Liu, L. (2014). Robust surface reconstruction via dictionary learning. In *ACM Transactions on Graphics*, page 201.

Zach, C., Pock, T., and Bischof, H. (2007). A globally optimal algorithm for robust TV-L 1 range image integration. In *ICCV IEEE International Conference on Computer Vision*, pages 1–8.